

¹ **The case for combining a large low-band VHF
2 transmitter with multiple receiving arrays for
3 geospace research: A Geospace Radar**

D. L. Hysell¹, J. L. Chau², W. A. Coles³, M. A. Milla⁴, K. Obenberger⁵, and
J. Vierinen⁶

¹Earth and Atmospheric Sciences, Cornell

University, Ithaca, NY, USA

²Leibniz-Institute for Atmospheric Physics

at the University of Rostock, Germany

³Electrical and Computer Engineering, U.C.

San Diego

⁴Jicamarca Radio Observatory, Instituto

Geofisico del Peru

⁵Space Vehicles Directorate, Air Force

Research Laboratory

⁶University of Tromso

Key Points.

1. A radar capable of probing a wide swath of Geospace could be assembled from a HPLA transmitter and a number of radio-array receivers.
2. Applications for such a geospace radar include MST, meteor, ionospheric, plasmaspheric, planetary, and solar research.
3. A geospace radar would promote discovery research and support space-weather applications.

4 We argue that combining a high-power, large-aperture (HPLA) radar trans-
5 mitter with several large-aperture receiving arrays to make a geospace radar -
6 a radar capable of probing near-earth space from the upper troposphere through
7 to the solar corona - would transform geospace research. We review the emer-
8 gence of incoherent scatter radar (ISR) in the 1960s as an agent which unified
9 early, pioneering research in geospace in a common theoretical, experimental,
10 and instrumental framework, and we suggest that a geospace radar would have
11 a similar effect on future developments in space-weather research. **We then dis-**
12 **cuss recent developments in radio-array technology that could be exploited**
13 **in the development of a geospace radar with new or substantially improved**
14 **capabilities compared to the radars in use presently. A number of appli-**
15 **cations for a geospace radar with the new and improved capabilities** are re-
16 viewed including studies of meteor echoes, mesospheric and stratospheric tur-
17 bulence, ionospheric flows, plasmaspheric and ionospheric irregularities, and re-
18 flection from the solar corona and coronal mass ejections (CMEs). We conclude
19 with a summary of technical requirements.

1. Introduction and motivation

20 The object of geospace science is to explore and understand humanity's place in the
21 solar system and the effects of variations in space on natural and technological systems.
22 This encompasses studies of processes in regions ranging from the surface of the Sun
23 through the interplanetary medium to the magnetosphere, radiation belts, plasmasphere,
24 ionosphere, and neutral atmosphere enveloping the Earth. Some of these processes are
25 detrimental to life and society and constitute space weather. The enormous scope of the
26 problem and the breadth of its impacts demand a comprehensive, integrated response from
27 multiple components of the scientific community working with a range of ground- and
28 space-based instruments, the agencies that support them, and the countries in which they
29 operate.

30 Similar comments would have been applicable at the start of the space age before the
31 fundamentals of plasma physics, in space and in the laboratory, were firmly established.
32 Scientists with a range of backgrounds struggled to understand the first observations of the
33 ionosphere from early spacecraft and from radio and radar apparatus designed for other
34 purposes in some instances, using different approaches and formalisms. A landmark event
35 in the history of space physics was the development in the 1960s of a theory to explain iono-
36 spheric scattering of signals transmitted from high-power, large-aperture (HPLA) radars.
37 What emerged, so-called "incoherent scatter theory," remains one of the most successful
38 applications of linear plasma theory to a complicated natural phenomenon and a textbook
39 example of how theory and technology can develop rapidly together. The legacy of the
40 era is a world-wide network of Incoherent Scatter Radars (ISRs) that remains the source

41 of the most incisive and least ambiguous measurements of ionospheric plasmas available
42 through remote sensing. Such radars are the centerpieces of the existing upper-atmospheric
43 facilities and are complemented by radio as well as optical ground-based instruments. The
44 upper-atmospheric facilities are well coordinated in the way they acquire, disseminate, and
45 interpret their observations.

46 While the last half century has seen tremendous advances in radio technology, signal
47 processing, and space-plasma theory, the ISRs function as much as they did in the early
48 days of development. They are configured mainly for monostatic operation, utilizing large
49 antennas or antenna arrays for transmission and reception. Beam steering, mechanical or
50 electronic, remains the paradigm for surveying large volumes. The radars operate at high
51 peak-power levels with relatively small duty cycles. Range resolution is enhanced mainly
52 through pulse coding and pulse compression. Radar frequencies have mainly been chosen
53 in the UHF band **for reasons having to do mainly with sky noise and licensing requirements.** Most of the ISRs concentrate their operating hours into specialized campaigns with
54 durations of a few days or weeks with low-power survey modes filling the gaps. **These**
55 **choices are rooted in history, including funding history and trends,** but are no longer
56 especially well suited for either scientific discovery or space-weather surveillance.

58 In this paper, we explore the outlines of the next generation of HPLA radars for geospace
59 research. The objective is to expand the coverage of the current radars to encompass a
60 larger segment of geospace. The central concept combines a main radio array for transmis-
61 sion with multiple, higher-resolution arrays for reception in the low VHF band, bridging
62 contemporary experimental principles from aeronomy and astronomy. The paper presents

63 a description of the current state of affairs, a discussion of the new capabilities modern ra-
64 dio arrays could provide, and a review of a few possible applications in geospace research.
65 Underlying the discussion is the premise that a geospace radar would serve the same inte-
66 grating role in the international space-physics community as the original ISRs that came
67 before them.

2. Conventional high-power, large-aperture radars

68 Starting with Arecibo in Puerto Rico and Jicamarca in Peru, the upper-atmospheric fa-
69 cilities were established to provide ground-based remote-sensing of near-Earth space to
70 complement observations coming from early spacecraft. The upper-atmospheric facilities
71 were built around pulsed HPLA radars to exploit the principle of incoherent scatter. In-
72 coherent scatter is modified Thompson scatter from fluctuations in free electron density in
73 a plasma. The relationship between the spectra measured by the radar and the state vari-
74 ables in the ionosphere is given by incoherent scatter theory [Salpeter, 1960; Fejer, 1960;
75 Dougherty and Farley, 1960; Farley *et al.*, 1961; Fejer, 1961; Hagfors, 1961; Salpeter,
76 1961; Rosenbluth and Rostocker, 1962; Dougherty and Farley, 1963; Perkins *et al.*, 1965;
77 Woodman, 1967]. In principle, incoherent scatter can be used to measure electron number
78 density, electron and ion temperature, ion composition, line-of-sight drifts, and collision
79 frequencies. The energetic electron population can also be inferred from the measure-
80 ments. Incoherent scatter theory becomes complicated in certain limits, notably for inci-
81 dence angles close to perpendicular to the geomagnetic field. Some aspects of the theory,
82 including the effects of Coulomb collisions on the spectra, are still topics of research and

83 further development [Kudeki and Milla, 2011; Milla and Kudeki, 2011]. Incoherent scat-
 84 ter is nonetheless the most direct and incisive technique we have for ionospheric remote
 85 sensing. Radars capable of incoherent scatter observations can presently be found in the
 86 United States and Canada, Peru, Scandinavia, Russia, Japan, and China. Other dual-use
 87 radars can be used for incoherent scatter such as the ALTAIR radar in the Kwajalein Atoll.

88 The upper-atmospheric facilities measure the most important state parameters in iono-
 89 spheric plasmas. Neutral parameters, including temperatures and winds, are not observed
 90 directly but can be inferred from the plasma measurements (e.g. Hysell *et al.* [2014]).

91 Higher-level ionospheric processes including chemistry, energetics, and transport can then
 92 be inferred from the state parameters through the application of conservation laws rooted
 93 in plasma kinetic or fluid theory. Nowadays, the conservation laws are typically encoded
 94 in computer models and simulations. Data from the upper-atmospheric facilities are ei-
 95 ther used for consistency checks for the models and simulations or incorporated directly
 96 through data assimilation. Data assimilation can be applied to very low-level radar data
 97 products, for example the spectra or autocorrelation functions of the signals themselves,
 98 avoiding some of the distortions inherent in estimating higher-level data products directly.

**The sensitivity of an ISR is partly governed by its figure of merit, f , the product of
 the transmitter average power in Watts and the effective antenna aperture in square
 meters divided by the product of the sky noise temperature in Kelvin degrees and the
 receiver bandwidth in Hz:**

$$f = \frac{PA}{BT} \quad (1)$$

99 The signal-to-noise ratio of a given experiment will generally be proportional to this
100 figure [Beynon and Williams, 1978]. Sensitivity also depends on other experimental
101 characteristics, however, including the sampling cadence (which can be enhanced by
102 exploiting frequency or polarization diversity) and the signal-processing strategy, and
103 so the figure of merit is not a comprehensive measure of overall ISR performance.
104 Another measure is the speed of an experiment which quantifies the time required
105 to achieve measurements with a given statistical accuracy [Lehtinen, 1986]. Still other
106 factors need to be considered when evaluating HPLA radar performance for dif-
107 ferent applications in geospace. Optimality exists within a complicated trade space
108 which has yet to be fully mapped.

109 Arecibo, which has the highest figure of merit of any of the ISRs, operates in the UHF
110 band near a minimum in the sky noise temperature. Jicamarca, meanwhile, operates at 50
111 MHz band where the sky noise temperature is two orders of magnitude greater (although
112 the bandwidth required is also an order of magnitude smaller). The low frequency is dis-
113 advantageous from the point of view of the figure of merit but advantageous in a number
114 of important ways.

115 One advantage of VHF, for example, is improved immunity from finite Debye-length
116 effects. The bandwidth of the ion line, the dominant incoherent scatter feature (at angles
117 away from the perpendicular to the geomagnetic field direction), is determined by the ion
118 rather than the electron thermal speed, but only if the the radar wavelengths λ is much
119 larger than the plasma Debye length. Measurements in rarefied plasmas necessitate long
120 radar wavelengths. Jicamarca has measured incoherent scatter to altitudes of about 10,000

₁₂₁ km and is also uniquely sensitive in the mesosphere where the electron number density is
₁₂₂ also small [Farley, 1991].

₁₂₃ Another property of the incoherent scatter spectrum is the drastic narrowing that occurs
₁₂₄ for incidence nearly perpendicular to the geomagnetic field. In this case, the spectrum be-
₁₂₅ comes much narrower than the ion thermal width, facilitating very accurate measurements
₁₂₆ of line-of-sight drifts. The phenomenon only occurs when $\lambda > 4\pi\rho_e$, where ρ_e is the elec-
₁₂₇ tron gyroradius, and can only be observed when the radar beamwidth is very narrow and
₁₂₈ the backscatter signal is dominated by the part coming from small magnetic aspect angles
₁₂₉ [Milla and Kudeki, 2011].

₁₃₀ Finally, high-power VHF radars can be used to study backscatter from fluctuations in
₁₃₁ the refractive index of neutral gases in the middle and lower atmosphere. MST radars are
₁₃₂ as important for studies of energetics, dynamics, and transport in the neutral atmosphere
₁₃₃ as incoherent scatter radars are in the ionosphere. With current technology and existing
₁₃₄ equipment, there need be no observing gap in altitudes between the boundary layer and the
₁₃₅ plasmapause.

₁₃₆ The existing ISRs employ vacuum tubes, traveling-wave tubes, klystrons, or transistors
₁₃₇ for RF power. The power source is lumped in the first three cases and distributed in the
₁₃₈ last case where transistors are typically situated very close to individual antenna elements.
₁₃₉ The conventional paradigm involves using pulsed transmitters with high peak-power levels
₁₄₀ and duty cycles ranging from a few percent to a few tens of percent. The duty cycle can be
₁₄₁ exploited to the greatest extent by using pulse compression schemes or pulse coding which
₁₄₂ allows long pulses to behave, in some respects, like shorter but more powerful pulses.

143 Pulse coding can also be used to make the radar instrument function or ambiguity function
144 closer to ideal, facilitating spectral measurements that are at once well resolved in range
145 and frequency. **Both random and deterministic pulse codes are in use at different ISRs**
146 **on the basis, in part, of the availability of signal generation equipment.** The price paid
147 for pulse compression is a reduction in sensitivity due to increased radar clutter. **Inverse**
148 **methodology is increasingly being used as a replacement for pulse compression in**
149 **some ISR applications (e.g. Hysell *et al.* [2008, 2017]).**

150 Today's ISRs utilize both phased-array and mechanically-steered dish antennas.
151 **Whereas the former allow for rapid steering, the latter can present attractive cost-**
152 **and performance-tradeoffs with respect to sidelobes and the ability to steer to low el-**
153 **evation angles.** Phased arrays also offer flexibility with regard to the use of spaced-antenna
154 methods, including interferometry and radar imaging. Subdividing the receive array for in-
155 terferometry and imaging comes at the cost of sensitivity and has been used in a limited
156 way with the two EISCAT ESR radars for studying the naturally-enhanced ion acoustic
157 lines (NIELS). Interferometry and imaging are used routinely for studying coherent scatter
158 with the modular phased array at Jicamarca.

159 The only multistatic ISR presently is the EISCAT mainland radar network which is
160 tristatic. Multistatic radars offer the ability to measure vector drifts unambiguously. Since
161 the EISCAT radars are mechanically steered, however, each scattering volume along the
162 transmit radar beam must be interrogated by the receive antennas one altitude at a time.
163 This seriously limits the cadence of experiments and the utility of the multistatic capabil-
164 ity.

3. Overview of radio arrays

165 A new paradigm for radio exploration of geospace comes from the **radio astronomy**
166 community where a new generation of radio arrays is being developed and deployed. The
167 radio arrays exploit spatial diversity to the fullest extent, going beyond traditional beam-
168 forming methods and utilizing all of the spatio-temporal information in radio signals from
169 subjects under study by using large-scale sparse interferometer systems. The geospace
170 radar concept involves combining radio arrays with discrete or distributed transmitters to
171 study volume scatter from the upper atmosphere and beyond. The goal is the production of
172 datasets which reveal the space-time structure of geospace phenomena unambiguously and
173 in a way that can readily be compared with or assimilated into numerical models, including
174 forecast models, as well as machine-learning algorithms.

175 Radio arrays have a long history in the arena of solar research. Reviewing some of the
176 milestones in this area provides context for the geospace-radar concept. The Culgoora
177 array consisted of ninety-six 13m-diameter mechanically steerable dishes, arranged in a
178 circle 3 km in diameter. It operated in dual polarization at 80 and 160 MHz. It was
179 designed for solar work and so did not attempt to suppress grating lobes so long as they
180 were out of the solar field of view. It was responsible for much of our understanding of
181 meter-wavelength radio bursts. The resolution was sufficient to measure scatter broadening
182 of Type III radio bursts by coronal turbulence.

183 In the case of the CLRO, the array was configured as a 3 km “T” of log-spiral antennas,
184 predominantly in a single circular polarization. It was designed for both solar and cosmic
185 work, so grating lobe suppression was important. It was one of the first to use a digital

₁₈₆ correlation receiver. Its resolution was comparable to Culgoora, but it covered a broader
₁₈₇ band with the log-spiral elements.

₁₈₈ In the last couple of decades, astronomical radio arrays have evolved significantly. The
₁₈₉ resolving capabilities of most modern radio telescopes are realized in two different ways:
₁₉₀ beamforming and interferometry. Perhaps the simplest way for a telescope to beamform is
₁₉₁ through the use of a dish (typically parabolic or spherical). Dishes are expensive, both to
₁₉₂ build and to maintain, and costs increase dramatically with the size of the dish. However,
₁₉₃ beamforming can also be accomplished using an array of dipoles, where the signal from
₁₉₄ each element is delayed and the total is coherently summed, effectively synthesizing an
₁₉₅ aperture. Historically, the delay portion of phased-array beamforming was accomplished
₁₉₆ with physical delay lines and phase-shifters which are awkward to calibrate and maintain.

₁₉₇ Unlike beamforming, interferometry by nature requires multiple elements. Voltage sam-
₁₉₈ ples from each element in an interferometer are cross correlated with the voltages from
₁₉₉ other elements. The physical distance and orientation of each antenna pair makes them
₂₀₀ sensitive to different spatial frequencies in different orientations. These spatial-frequency
₂₀₁ measurements can be Fourier transformed and summed to form an image. This process is
₂₀₂ called synthesis imaging as the elements in the array are synthesizing points on an aperture.
₂₀₃ For an interferometer comprised of N elements, there are $N \times (N - 1)/2$ unique cross-
₂₀₄ correlation products. Although phase shifting can be performed after the cross-correlation,
₂₀₅ delay compensation is necessary in broadband systems, and this remains awkward and
₂₀₆ expensive. In the past, the fact that the computational load increased like the number of
₂₀₇ elements squared prohibited many-element interferometers.

208 Recently, advancements in computational power have opened the door to both digital
209 beamforming and large- N synthesis imaging. In particular, large arrays comprised of hun-
210 dreds of dipoles can digitally steer multiple beams simultaneously across large bandwidths
211 using off-the-shelf CPUs **and, in practice, GPUs**. **The adoption of GPUs** by the radio
212 astronomy community has allowed for real-time, wide-band synthetic imaging with fields
213 of view limited only by the beam pattern of an individual antenna elements. Delays are
214 still necessary, but they simply imply a digital buffer. Furthermore, digital buffers can
215 be large enough to store the entire RF signal for the duration of an event so that, when
216 an event is detected, the entire buffer can be saved and reprocessed as necessary. Such
217 an event might be a fast radio burst (FRB) in radio astronomy, but many such situations
218 can also be imagined in geospace research. These advancements are revolutionizing radio
219 astronomy, but the geospace and space-weather communities for the most part continue
220 to use decades-old facilities that rely on single dish or delay-line technology. **Below, we**
221 **highlight radio arrays that are changing the trend and being exploited for pioneering**
222 **geospace research.**

223 **LOFAR:** The Low Frequency ARray (LOFAR), the largest radio telescope in the lower
224 VHF band, was built and is operated by the Netherlands Institute for Radio Astronomy,
225 ASTRON. LOFAR is comprised of individual stations, most of which are located in the
226 Netherlands. Currently, there are 24 core stations located in Exloo, NL, 14 remote stations
227 located across the Netherlands, and 12 international stations located across Europe. Each
228 station includes both low band (10-80 MHz) and high band (120-240 MHz) arrays.

229 The low band antennas consist of two linear, orthogonal dipoles, each made of two cop-
230 per wires. The dipoles are resonant at 60 MHz and drop in sensitivity away from this
231 frequency. The low band arrays of the core and remote station include 48 low band an-
232 tennas, and the international stations include 96. Beamforming with an individual station
233 is done electronically, allowing for fast beam steering with no moving parts. The beam-
234 formed time series are then sent to a correlator for high-resolution imaging [*van Haarlem*
235 *et al.*, 2013].

236 **KAIRA:** The Kilpisjärvi Atmospheric Imaging Receiver Array (KAIRA) is a LOFAR
237 station which was constructed in 2011 in Northern Finland. KAIRA has demonstrated suc-
238 cessfully that modern, low-frequency, digital phased array radio telescopes can be highly
239 versatile instruments for studying various geophysical phenomena in Earth’s near space
240 using radio remote sensing [*Vierinen et al.*, 2013; *McKay-Bukowski et al.*, 2015]. The fre-
241 quency range of $\approx 10 - 240$ MHz is ideal for studies of the Earth’s near space. At these
242 frequencies, the radar cross-sections of mesospheric echoes, meteor trail, and head echoes
243 are maximized. As stated above, lower frequencies also allow observing lower plasma
244 densities due to Debye-length effects. At lower frequencies, radio propagation effects such
245 as scintillation and absorption are also stronger, facilitating studies of these phenomena.

246 Due to the versatile nature of the underlying digital phased array technology, the same
247 system can be used for a number of different active and passive geophysical radio remote
248 sensing applications including phased array incoherent scatter radar [*Vierinen et al.*, 2013;
249 *Virtanen et al.*, 2014], spectral riometry [*Kero et al.*, 2014], multi-static studies of the meso-

250 sphere [*Chau et al.*, 2018a], and for characterization of wide-band ionospheric scintillation
251 [*Fallows et al.*, 2014].

252 One of the strengths of the all-digital phased array technology is the wide bandwidth.
253 This allows multi-wavelength studies of various plasma physics phenomena in geospace.
254 The refractive index for ionospheric plasma is frequency dependent. The same applies for
255 radar cross-sections of various phenomena such as meteor head echoes and mesospheric
256 echoes. So far, the information from simultaneous, multi-wavelength observations has
257 remained relatively unexplored. Due to the wide band nature, KAIRA can actually be
258 used together with multiple radar transmitters as a phased array radar receiver. So far,
259 it has been used together with the EISCAT VHF transmitter, the MAARSY MST radar,
260 and the Andøya meteor radar. Therefore, another strength of using modern radio arrays is
261 that they can be used together with a range of existing and planned radar transmitters as a
262 multi-static platform.

263 **MWA:** The MWA consists of 2048 dual-polarization dipole antennas optimized for the
264 80-300 MHz frequency range, arranged as 128 “tiles”, each a 4×4 array of dipoles. The
265 array has no moving parts, and all telescope functions including pointing are performed by
266 electronic manipulation of dipole signals, each of which contains information from nearly
267 four steradians of sky centered on the zenith. Each tile performs an analog beamforming
268 operation, narrowing the field of view to a fully steerable 25 degrees at 150 MHz.

269 The majority of the tiles (112) are scattered across a roughly 1.5 km core region, form-
270 ing an array with very high imaging quality, and a field of view of several hundred square
271 degrees at a resolution of several arcminutes. The remaining 16 tiles are placed at loca-

272 tions outside the core, yielding baseline distances of about 3 km to allow higher angular
273 resolution for solar burst measurements.

274 Important ionospheric research has already been performed with the MWA. In particular,
275 *Loi et al.* [2015] recently identified field-aligned ionization ducts between the ionosphere
276 and the plasmasphere in spatially-resolved maps of total electron content (TEC).

277 **LWA:** The Long Wavelength Array (LWA) is a concept for an HF/VHF radio tele-
278 scope comprised of 52 stations spread over the state of New Mexico, providing 0.4 km^2 of
279 collecting area. With baselines ranging from a few km up to about 400 km, such a radio
280 telescope could achieve down to 5 arc second resolution.

281 A single LWA station is comprised of 256 dual polarization, bow tie antennas pseudo-
282 randomly spread over a 100x110 m ellipse. The antennas are slightly bent to achieve
283 greater sensitivity to a wider range of zenith angles. A single station can act as a 256-
284 element interferometer, capable of imaging nearly the entire visible sky, or as a digital
285 beamformer, capable of producing several beams at once.

286 To date, two stations have been completed in New Mexico. The first station, LWA1,
287 is collocated with the Very Large Array and operates from 10-88 MHz [*Ellingson et al.*,
288 2012]. The second station, LWA-SV, which is located at Sevilleta National Wildlife refuge,
289 is operationally nearly identical to LWA1 except it has modified analog filters allowing
290 observations down to 3 MHz.

291 Furthermore, the digital processor on LWA-SV has been upgraded from LWA1 to make
292 use of graphics processing units (GPUs) through the Python/C++ Framework known as
293 Bifrost [*Cranmer et al.*, 2017]. GPUs are capable of performing large numbers of ba-

294 sic calculations simultaneously, making them ideal for radio arrays comprised of many,
295 non-uniformly distributed elements such as an LWA station. Bifrost is designed to work
296 on streaming data such as radio array voltages in real time and allows for rapid pipeline
297 development with its high-level python interface.

298 LWA at Owens Valley Observatory (LWA-OVRO) is a higher resolution LWA telescope
299 built for monitoring of astrophysical transients. With maximum baselines of 100 m, LWA1
300 and LWA-SV achieve a synthesized beam full width at half the maximum (FWHM) of a
301 few degrees in the lower VHF band. However with maximum baselines of 1.5 km, LWA-
302 OVRO is capable of imaging the entire sky at a resolution of a few 10s of arcmin.

303 **EISCAT_3D:** EISCAT 3D is a next generation all-digital multi-static phased array
304 radar which is currently being constructed in Northern Scandinavia [McCrea *et al.*, 2015].
305 The core transmit-receive site will be located in Skibotn. Two outlier receive-only system
306 are to be located in Sweden and Finland, approximately 150-km distance from Skibotn.
307 Each one of the sites consists of 109 modules, with 91 antennas in each module. The
308 operating frequency is 233 MHz. The transmit power will be 5 MW peak power with a
309 25% duty-cycle.

310 The main novelty of EISCAT 3D is that it will have the capability of observing vector
311 ion velocities simultaneously at all altitudes by using multiple bistatic beams that intersect
312 the transmit beam. Due to the rapid beam switching capability, the radar will be able to
313 perform a volumetric observation quickly. EISCAT 3D will also enable aperture-synthesis
314 radar imaging in order to improve spatial resolution of auroral radar observations, a tech-

³¹⁵ nique that has been used already for a long time at the Jicamarca Radio Observatory (e.g.
³¹⁶ *Hysell and Chau [2006]*).

³¹⁷ Once finished, EISCAT 3D will be the most modern incoherent scatter radar in the world.
³¹⁸ By virtue of its frequency and its latitude, it will not, however, be able to fulfill all of the
³¹⁹ objectives of a geospace radar as laid out in this paper. Unlike LWA or LOFAR, the EIS-
³²⁰ CAT 3D receiver array is also relatively narrow band (30 MHz), limiting the applicability
³²¹ of the radio array for uses other than 233-MHz radar operations.

4. Capabilities of modern radio arrays paired with HPLA transmitters

³²² In this section, we summarize some of the existing and potential capabilities that modern
³²³ radio arrays would bring to geospace research operating in radar mode, particularly in
³²⁴ the low-VHF band. To keep our summary focused, we assume a large radio array for
³²⁵ transmission and multiple, spatially separated radio arrays for reception. In this respect,
³²⁶ we start with the transmitting capabilities and continue with the receiving capabilities and
³²⁷ the motivation for focusing on the low-VHF band.

4.1. Transmitter capabilities

³²⁸ Recent developments in technology allow the possibility of large transmitting arrays
³²⁹ with solid-state transmitters possibly at each antenna element. Solid-state technology in
³³⁰ conjunction with contemporary, compact antenna element designs (e.g., LWA), would al-
³³¹ low operations over a relatively broad band at low VHF frequencies. Moreover, modern
³³² designs would allow larger duty cycles and even continuous wave (CW) operation. This

333 implies an increase in average power even for systems that are peak-power limited. The
334 result is the ability to probe a broader range of geospace.

335 Although performance advantages of a distributed transmitter are clear, radar users are
336 well-aware that much of the costs of operating a radar are in operating and maintaining
337 the transmitter. It is this that limits the operating hours of many ISRs. By comparison,
338 a distributed transmitter **might be expected to pose fewer maintenance challenges over**
339 **time** and permit 24/7 operation at little additional cost.

340 The possibility of a transmitter on each antenna, and depending on the RCS of the desired
341 target, allows:

- 342 • Fast beam steering to reduce space-time ambiguity.
- 343 • Multiple, simultaneous beam pointing directions for multi-target, multi-use applica-
344 tions [*Milla et al.*, 2013].
- 345 • Antenna compression to generate beams with different widths [*Woodman and Chau*,
346 2001; *Chau et al.*, 2009].
- 347 • Implementation of multi-frequency approaches to improve range resolution (range
348 imaging).
- 349 • Implementation of coherent MIMO configurations using code diversity [*Urco et al.*,
350 2018]. Coherent MIMO can be used to take advantage of the spatial information arising
351 from distributed transmitter modules .
- 352 • Implementation of low-power modes, either for long-term operations or for strong
353 targets.

354 In the last 10 years, great progress has been made with **broadband** phased array radio
 355 telescopes. There would be great benefit from a matching frequency-agile transmit capabil-
 356 ity. This would allow radar studies of space plasma physics phenomena with one additional
 357 independent variable: frequency. This information would be useful, e.g., for studies of at-
 358 mospheric turbulence spectra and determining the sizes of meteor head echoes. For solar
 359 radar, this would allow studies of the solar corona at different depths [Bastian, 2003, 2004].

4.2. Receiver capabilities

360 In the case of receivers, based on the recent developments in radio astronomy (e.g.,
 361 LOFAR, LWA), monostatic and multistatic configurations would provide significant new
 362 capabilities to a geospace radar. Much like a radio telescope, a geospace radar receiver
 363 could leverage the power and flexibility of software controlled beamforming and aperture
 364 synthesis imaging. Furthermore, a radio astronomy-like digital processor could easily be
 365 modified for flexible radar processing and data acquisition. This has already been demon-
 366 strated with LOFAR [Vierinen *et al.*, 2013] and LWA [Taylor, 2014].

367 The new capabilities for reception, related to the transmitter capabilities described above
 368 but not limited to them, would include:

- 369 • Many simultaneous independent beam pointing directions available at all times. This
 370 allows, e.g., different altitudes to be sampled simultaneously by a multistatic receiver and
 371 many other presently impossible operational modes.
- 372 • Multistatic reception capability for resolving three-dimensional flows unambiguously.
- 373 • Antenna compression to generate beams with different widths on reception.

374 • Implementation of synthetic aperture imaging by utilizing smaller sections within re-
375 ceiving arrays or combining spatially separated receiving arrays (e.g., LOFAR core).

376 • Implementation of coherent MISO, i.e., single antennas (or group of antennas) could
377 be used for interferometric/imaging purposes if the target is sufficiently strong.

378 • Broadband interference identification and rejection from sources such as lightning
379 and solar radio bursts.

380 The theme of these capabilities is the exploitation of spatial diversity to resolve features
381 and flows in three dimensions, expanding the domain of geospace radar observations be-
382 yond simple profiling and conventional monostatic beam forming. The applications iden-
383 tified below exemplify the need for the capabilities specifically.

4.3. Why low-band VHF?

384 **There are clear disadvantages associated with operating in the VHF band. Lower**
385 **frequencies imply larger array sizes, greater material costs, and greater demands**
386 **on real estate. Licensing in the VHF band may also be difficult in some countries. Most**
387 **importantly, increased galactic noise at VHF compared to UHF implies challenges for**
388 **system sensitivity and a potential requirement for greater transmitter power. The sen-**
389 **sitivity problem is mitigated partly by reduced atmospheric absorption and cabling**
390 **losses.**

391 Despite these problems, most of the geospace-radar applications above would benefit
392 from using low-band VHF. In terms of feasibility, the technology needed for a low-band
393 VHF geospace radar is already proven; the required antennas, digital receivers, beam for-
394 mers (based on FPGA), and solid-state transmitters are available commercially now. A

395 number of other factors make low-band VHF advantageous. For example, radio frequency
 396 interference (RFI) in the low band VHF can be a limiting factor for receiving arrays. How-
 397 ever, as shown by both LOFAR [*van Haarlem et al.*, 2013] and LWA1 [*Ellingson et al.*,
 398 2012], the spectrum between 30 and 80 MHz is relatively clean, even in densely populated
 399 countries like the Netherlands. Other noteworthy factors related to low-band VHF radar
 400 are summarized in the following list:

- 401 • Radio propagation effects of interest such as Faraday rotation and scintillation are
 402 stronger at low VHF frequencies.
- 403 • Array element patterns are broader in the low VHF band. This allows any fully-digital
 404 low-band receiving array to have an unlimited number of beams covering the entire visible
 405 hemisphere at no penalty in signal-to-noise ratio.
- 406 • The radar cross-sections of many of the phenomena of interest are also larger.
- 407 • Finite Debye-length effects for ISR impose less severe limitations on the minimum
 408 detectable electron number density.
- 409 • Planetary (Lunar) studies would benefit from deeper subsurface penetration at VHF.
- 410 • The power spectral density of galactic synchrotron emission as a function of fre-
 411 quency is proportional to $f^{-2.5}$ [*Rogers and Bowman*, 2008]. However, the bandwidth
 412 of the incoherent scatter ion line, and therefore the minimum receiver noise bandwidth,
 413 is proportional to f . This means that the signal to noise ratio for the ion-line is not as
 414 strongly dependent on frequency as one would expect by just looking at the sky noise:
 415 $\text{SNR}(f) \propto f^{1.5}$.

5. Geospace radar applications

416 In this section, we describe some of the possible applications of a new geospace radar,
417 starting from the lower atmosphere and ending at the Sun. The applications are meant to be
418 illustrative rather than exhaustive. New applications will emerge as novel remote sensing
419 approaches designed for the current applications mature.

5.1. MST applications

420 The neutral atmosphere can be also studied with VHF radars in so-called MST mode.
421 The first application of such radars for neutral atmospheric dynamics was conducted at
422 Jicamarca [Woodman and Guillén, 1974]. Since then, the MST technique proliferated
423 world-wide, with small systems covering the altitudes between a few hundred meters to
424 lower stratospheric altitudes (i.e., less than 20 km). The altitudinal coverage of these sys-
425 tems depends on the frequency of operation, size of the antennas, and transmitting power.
426 The corresponding systems are called boundary layer radars, wind profilers, and ST radars
427 [Hocking, 2011]. In the case of the mesosphere, there is a handful of HPLA radars work-
428 ing between 45 and 55 MHz, able to receive echoes from irregularities embedded in neu-
429 tral turbulent layers (e.g., Jicamarca, Gadanki, MU, MAARSY). At high latitudes, due to
430 the presence of charged ice particles during the summer, smaller systems are being used
431 to study the polar summer mesosphere from so-called polar mesospheric summer echoes
432 (PMSE). In all these cases, low VHF frequencies have been used to study the neutral at-
433 mosphere from a few hundred meters to the lower stratosphere and in some parts of the
434 mesosphere depending on the latitude, time of the day, and season.

435 The region between the lower stratosphere and the lower mesosphere (i.e., between 20
436 and 55 km) has been known as the “radar gap region” since this region typically cannot
437 be observed with existing radars. Using long integration times and dual polarizations at
438 Jicamarca, *Maekawa et al.* [1993] reported on atmospheric echoes from this region for the
439 first time.

440 A modern and powerful geospace radar should be able to sample the whole MST re-
441 gion by combining low-power modes for the lower atmosphere with high-power modes
442 for the stratosphere and mesosphere. The stratosphere and lower mesosphere is the region
443 where primary gravity waves are expected to break and dissipate, modify the background
444 conditions, and generate so-called secondary gravity waves.

445 The daytime exploration of the mesosphere could be also complemented with ISR obser-
446 vations of the D region. Although radar scattering is from electrons, the collision frequency
447 at these altitudes is so high that the dynamics of the measured spectra are dominated by the
448 neutrals. Using the Poker Flat Incoherent Scatter Radar (PFISR) during a strong auroral
449 precipitation event, *Nicolls et al.* [2010] were able to study inertial gravity waves that had
450 originated a few days before at the surface a few thousand kilometers away. In the case of
451 a powerful geospace radar, such atmospheric events could be studied during the daytime
452 routinely, i.e., without the need of strong electron density enhancements.

453 Besides exploring a new altitudinal region, a modern geospace radar could be used to
454 explore the MST region with larger horizontal coverage and greater altitudinal, horizon-
455 tal, and temporal resolution than is presently possible. Such improvements would allow
456 the combination of radar imaging, range imaging, multi-static observations, and MIMO

implementations. Recently, *Urco et al.* [2019] observed PMSE with unprecedented horizontal resolution using a combination of Maximum Entropy and MIMO techniques. The resolution achieved with the MAARSY 90-m diameter antenna was equivalent as to having a 450-m diameter array. The resulting images show that the summer polar mesosphere presents rich spatial and temporal structures associated to a combination of vertically propagating waves from below, horizontally drifting waves, and instabilities and waves generated in situ. Figure 1 shows an example of such 3D images obtained with 40 second integrations: (a) a horizontal cut at 85.80 km, (b) an altitude vs zonal direction cut, and (c) an altitude vs meridional cut, color-coded with Doppler velocity, spectral width and intensity information. A powerful geospace radar would allow similar mesospheric observations at low and middle latitudes where mesospheric echoes are mainly dependent on atmospheric turbulence and therefore have an RCS a couple of orders of magnitude smaller than PMSE.

The horizontal coverage can be extended, in the case of lower atmospheric altitudes where the echoes are stronger, by using smaller sections of the transmitter array, different pointing directions, and multi-static configurations.

5.2. Meteor science and applications

In the mesosphere and lower thermosphere (MLT), i.e., between 70 and 120 km, echoes from meteors can be also observed with low VHF-band radars. There are three main types of meteor echoes: (a) specular trail echoes due to Fresnel scattering when the radar points perpendicular to the meteor trajectory, (b) Head echoes coming from plasma as it forms in front of the meteoroid, and (c) non-specular trail echoes, also known as range-spread

477 trail echoes resulting from the combination of field-aligned irregularities and charged dust
478 particles.

479 Meteor echoes have been used to study meteoroid composition, origin, and masses, and
480 to explore the MLT region. Traditional specular meteor echoes have been used since the
481 1950s to explore the MLT dynamics with small radars systems called specular meteor
482 radars (SMRs). They are typically composed of one wide-beam transmitting antenna and
483 a receiver interferometer operating between 30 and 50 MHz. Recently, such systems have
484 been improved using multi-static geometries, coded CW transmissions, and MIMO con-
485 figurations [Stober and Chau, 2015; Vierinen *et al.*, 2016; Chau *et al.*, 2018b]. The im-
486 provements allow such systems to measure the MLT wind fields with much larger horizon-
487 tal coverage and resolution as well as improved vertical and temporal resolutions [Stober
488 *et al.*, 2018]. Current efforts are being devoted to determining the second order statistics
489 of the wind field as function of wavenumber (horizontal and vertical) as well as frequency.

490 A powerful geospace radar would allow the detection of much weaker signals due to
491 meteoroids with less mass or smaller entry speeds. One of the outstanding questions in
492 aeronomy is how much meteor mass is deposited in the atmosphere? So far, different
493 methods provide estimates with a couple of orders of magnitude spread. A geospace radar
494 could greatly improve the measurements of the lower mass/speed end of the spectrum,
495 from both head as well as specular meteor echoes.

496 In the case of head echoes, only HPLA radars with interferometry are able to determine
497 precisely the meteoroid trajectory and where in the beam such echoes occur, something
498 crucial for the scattering meteor mass determination. So far, such measurements have been

499 conducted only at Jicamarca, MU, and MAARSY using narrow beam configurations [*Chau*
500 *et al.*, 2007; *Kero et al.*, 2011; *Schult et al.*, 2017]. The use of a wider beam, longer duty
501 cycle sequences, and MIMO configurations would improve significantly the detection and
502 characterization of such echoes.

503 Non-specular meteor echoes are still enigmatic since they appear to result from a com-
504 bination of field-aligned irregularities and charged dust particles. A clear indication of the
505 former comes from observations at low and mid latitudes where these relatively long-lived
506 range-spread echoes come primarily when the beam points perpendicular to B . The latter
507 come from high latitude observations where perpendicular-to- B observations are not possi-
508 ble. Besides the interest in understanding the physics behind these echoes, they can be used
509 to get precise altitudinal profiles of MLT winds with high temporal and spatial resolution
510 [*Oppenheim et al.*, 2009]. The proposed geospace radar, if located at low or mid latitudes,
511 would be able to provide such measurements on routine basis, contributing further to the
512 complicated atmospheric dynamics of the MLT region. Besides routine observations of
513 these profiles, the horizontal coverage would be improved by using multi-static and multi-
514 beam approaches.

5.3. Ionospheric research

515 Since its inception, the incoherent scatter technique has provided the most incisive mea-
516 surements of ionospheric state parameters available through ground-based remote sensing.
517 These include plasma number densities, temperatures, composition, and line-of-sight drifts
518 as well as information about the electron energy distribution and inferences about the state
519 of the neutral atmosphere. Most of the information has come in the form of profiles ob-

520 tained along the beam pointing direction of the radar. Profiles are useful in view of the fact
521 that the ionosphere is vertically stratified. Volumetric information came mainly from me-
522 chanical beam steering before the emergence of the Advanced Modular Incoherent Scatter
523 Radars (AMISRs) currently deployed in Alaska and Canada which employ electrically-
524 steered phased arrays.

525 The importance of obtaining volumetric information is highlighted by Figs. 2 and 3
526 which represent radar observations of plasma density irregularities associated with plasma
527 convective instability at low magnetic latitudes and so-called “equatorial spread *F*.” Fig. 2
528 was obtained by the ALTAIR radar in the Marshall Islands and shows an east-west scan
529 acquired at pointing angles a few degrees away from perpendicular to the geomagnetic
530 field. The figure exhibits large-scale undulations in the *F*-region bottomside along with
531 depletion plumes penetrating through the *F* peak and into the topside. The irregularities
532 evolve on timescales of a few minutes or tens of minutes which is comparable to the time
533 required to complete a scan. Although informative, the figure is not a true image and is
534 highly distorted.

535 Fig 3 shows data acquired a few minutes earlier along antenna pointing positions pre-
536 cisely perpendicular to the geomagnetic field. Patches of intense backscatter concentrated
537 in the depleted regions in Fig. 2 represent coherent scatter or Bragg scatter from small-
538 scale field-aligned plasma density irregularities. Like the large-scale irregularities evident
539 in Fig. 2, the small-scale irregularities are a consequence of plasma instability and signify
540 the presence of free energy in the ionosphere. They are a vivid manifestation of space

541 weather and a hazard for radio communication, navigation, and imaging systems operating
542 at low geomagnetic latitudes.

543 The coherent scatter conveys information about the the underlying plasma instabilities
544 that is highly complementary with the incoherent scatter which conveys information about
545 plasma state variables. Ideally, we would like to acquire signals from the entire ionospheric
546 volume within the figure simultaneously, including from both large and small magnetic
547 aspect angles. This would be true imaging and would permit direct, unambiguous compar-
548 ison with direct numerical simulations.

549 One of the major shortcomings of the ALTAIR data in Figs. 2 and 3 is the absence
550 of reliable drifts measurements. Plasma drifts at the geomagnetic equator are relatively
551 small, and the incoherent integration time necessary to acquire and formulate accurate
552 drifts measurements in this case is longer than the timescale along which the large-scale
553 plasma irregularities evolve. The measurement is not stationary at UHF frequencies. At
554 low VHF frequencies, and for beam pointing angles very close to perpendicular to the
555 magnetic field, accuracy of ISR drifts measurements improves dramatically, and the mea-
556 surements become stationary. This is a strong argument for favoring low VHF frequencies
557 for a geospace radar.

558 The high quality of ISR drifts obtained with beams pointing perpendicular to the mag-
559 netic field is due to the narrowness of the ISR spectrum at low VHF frequencies allowing
560 the application of Doppler-shift detection to estimate the drifts. The narrowness of the
561 spectrum is caused by the relatively long temporal correlation of the field-aligned electron
562 density fluctuations that diffuse slowly across the magnetic field lines. Such diffusion is

563 not dominated by Landau damping but by Coulomb collisions. Incoherent scatter theory
564 has been reformulated recently to incorporate the effects of Coulomb collisions on particle
565 dynamics by describing the statistics of electron and ion trajectories using a Fokker-Planck
566 kinetic equation with speed-dependent friction and diffusion coefficients. Measurements
567 with the Jicamarca radar at 50 MHz have been shown to agree with the proposed theory.
568 However, the validation is limited since only a single radar frequency has been used in a
569 particular configuration. A modern geospace radar would let us to conduct similar tests to
570 study the effects of Coulomb collisions on ISR signals at multiple radar frequencies, mag-
571 netic aspect angles, and antenna beam widths for different ionospheric altitudes including
572 topside regions where plasma composition would impose another level of complexity. This
573 study is of general relevance as a test for theoretical plasma physics.

5.4. Plasmaspheric research

574 A problem was discovered recently with the standard high-altitude ISR mode at Jica-
575 marca. Samples acquired from very high altitudes were being used as the basis for noise
576 estimates. From time to time, however, the noise estimates became contaminated. Upon
577 closer examination, the contamination was found to be due to coherent scatter from high
578 altitudes just above 2000 km. This is the altitude where the on-axis antenna pointing
579 position at Jicamarca was perpendicular to B at the time. High-altitude field-aligned irreg-
580 ularities were the cause. The irregularities occurred mainly in the pre-dawn sector. The
581 immediate problem was solved by using samples taken during transmitter-off intervals for
582 noise estimates. The problem of the origin of the high-altitude field-aligned irregularities
583 remains.

584 An example of the phenomenon in question is shown in Fig. 4. The figure was generated
585 by computing the modulus of the longest lag in the measured ISR lag-product profiles, 1.5
586 ms, which should be essentially zero for incoherent scatter. The experiment in question is
587 very sensitive compared to more conventional coherent scatter experiments, and the echoes
588 were not very strong compared to what is received from the electrojet or equatorial spread
589 *F*. The coherent scatter occurred in layers that migrated in altitude slowly in time. Since
590 the experimental geometry favored field-aligned echoes between about 2000-2500 km in
591 this case, we do not know the true altitude span of the irregularities.

592 Subsequent discussions revealed that this phenomenon had been known since the earliest
593 days of Jicamarca (personal communication, D. T. Farley, J. P. McClure). However, it was
594 not deemed to be as interesting as the other ionospheric phenomena being discovered in
595 the 1960s and was never pursued. Contemporary ISR experiments designed to remove
596 outliers arising from different kinds of radar clutter masked the phenomenon which was
597 only rediscovered by accident.

598 The high-altitude coherent scatter is significant since it signifies the presence of an un-
599 known source of free energy and an unknown plasma instability. The echoes are not merely
600 high-altitude examples of FAIs caused by equatorial spread *F* which can occur above 2000
601 km altitude during periods of high solar flux under geomagnetically-disturbed conditions.
602 The echoes in Fig. 4 occurred during a period of low solar flux and quiet conditions.
603 They were not preceded by spread *F* and occurred during June solstice when spread *F* is
604 relatively uncommon. That they occur mainly in the pre-dawn sector suggests that beam

605 instabilities driven by photoelectrons may be playing a role. To test the hypothesis, dedicated
606 rather than serendipitous observations are required.

5.5. Planetary research

607 Low frequencies are especially useful for probing the subsurface of dielectric bodies.
608 The penetration depth of an electromagnetic field is inversely proportional to frequency.
609 Lower frequencies are used in Earth remote sensing for applications such as hydrology
610 and foliage-penetrating radar. In the case of planetary exploration, low frequency observa-
611 tions are used to probe the subsurface of planetary bodies, e.g., in search of subsurface ice
612 deposits on Mars or ice on permanently shadowed craters on the Moon. In general, radar
613 observations across a number of different frequencies can yield a great deal of information
614 on the geological surface and subsurface composition and structure of planetary bodies.

615 With a geospace radar, the only planetary body that can be mapped with good resolution
616 is the Moon. The Moon is close enough that high signal-to-noise ratios can be achieved. It
617 is also large enough that the target size in range and Doppler shift permits a large number
618 of measurement points. Contemporary 6-meter wavelength radar mapping efforts achieved
619 approximately a 15x15 km resolution which is limited by ionospheric scintillations and the
620 limited tracking time possible. With a more flexible low frequency radar, it is plausible to
621 obtain range-Doppler resolution of approximately **1.5 km × 1.5 km** per pixel with good
622 ionospheric conditions from a non equatorial location.

623 A low frequency polarimetric inverse synthetic aperture radar image of the Moon ob-
624 tained at Jicamarca [Vierinen *et al.*, 2017] is shown in figure 5. This 49.92 MHz radar
625 image is the lowest frequency polarimetric synthetic aperture map of the Moon that has

626 been made, allowing us to peer deeper beneath the surface of the Moon than before. This
627 frequency is close to the lowest possible frequency that can be used for a ground based ob-
628 servation due to deleterious effects of ionospheric scintillation and other radio propagation
629 effects.

630 The 6-meter wavelength radar map provides a unique view of the Moon. Resonant
631 scattering from Breccia in the vicinity of newer impact craters allows us to infer the amount
632 of large blocky material. These regions appear radar bright. Examples of such regions
633 include the area in and around the Copernicus and Tycho craters. The bulk radar brightness
634 on the other hand allows us to infer the dielectric properties of the subsurface. Lossy FeO
635 and TiO₂ rich mare regions of the Moon have a larger loss tangent and appear radar dark
636 while low loss terrae regions appear radar bright.

637 One of the key findings of the 6-meter wavelength study [Vierinen *et al.*, 2017] was the
638 discovery of a large radar dark region which joins Mare Frigoris and Mare Imbrium. This
639 finding supports the hypothesis that Mare Imbrium and Mare Frigoris are part of the same
640 impact basin – one of the largest impact basins on the Moon. The other key finding was
641 the radar dark Schiller-Zucchius impact basin on the southern hemisphere of the Moon.
642 This can be seen on the top-right panel of Figure 5. The radar observation supports the
643 hypothesis that this old impact basin is associated with basaltic flows which are now mostly
644 covered by optically bright terrae material produced by newer impact ejecta. These recent
645 findings show that low frequency planetary radar, which peers beneath the visible surface
646 of the Moon, can provide important new information about the geological formation of the
647 Moon which is still poorly understood.

5.6. Solar research

648 The cause celebre for geospace radar could well be solar research. The ability to receive
649 soundings from the sun with ground-based radar would represent a new avenue for study-
650 ing solar physics. It could expedite the creation of an operational space-weather forecast
651 strategy involving tracking along with prediction of CME trajectories. Finally, it would
652 unify the solar, magnetospheric, and ionospheric research communities under a common
653 observational paradigm. The concept is not new and is not simple but appears to be plau-
654 sible using available dual-use technology.

655 **5.6.1. Historical background**

656 Since the start of the planetary-radar era, multiple attempts have been made to detect
657 radar reflections (soundings) from the solar corona. The first, in 1959, was by a Stanford
658 University group working at 25.6 MHz [*Eshleman et al.*, 1960]. Eshleman reported detect-
659 ing echoes at 1.7 solar radii after 36 min. of integration using a monostatic radar system
660 with 25 dB of antenna gain and 40 kW average power. The results were deemed to be
661 consistent with expectations for an ideal, conducting sphere at the time but could not be
662 repeated.

663 Subsequently, a major, multi-year effort was undertaken by a group from MIT using a
664 dedicated 38.25 MHz radar built in El Campo, Texas [*James*, 1964, 1970] and operated
665 continuously from 1960 to 1969. The average power and gain of the El Campo radar
666 were 500 kW and 33–36 dB, respectively. These are very impressive specifications for
667 what would be a temporary, short-lived radar facility. Highly variable echoes (in terms
668 of power, Doppler shift, and bandwidth) were reported. Several analysts attributed the

669 variable echoes not to critical-frequency reflection but to coherent scatter from one or more
670 electrostatic plasma waves (e.g. [Khotyaintsev, 2005]). Despite the unexpected variability
671 of the signals, at the time and for decades thereafter, the El Campo results were considered
672 to be reliable and definitive if not particularly well documented proof of the solar-radar
673 concept. **The results have not been replicated, in part due to the absence of a suitable**
674 **facility for performing the experiments.**

675 Another attempt was made at Arecibo in 1966 and 1967, using a 40-MHz, 50/100 kW
676 average power transmitter [Parrish, 1968]. The gain of the Arecibo system at 40 MHz was
677 37 dB. The investigators duplicated the experimental mode utilized earlier at Stanford.
678 While preliminary work suggested that solar echoes were detectable, and while positive
679 results were again obtained when the experiments were repeated, the results were never
680 published. The perceived lack of novelty rather than any shortcomings in the research kept
681 the results from the literature (D. Campbell, 2016, personal communication.) The 40-MHz
682 transmitter was decommissioned, and no further attempts have been made at Arecibo.

683 In 1996, solar radar experiments were attempted in the FSU using the SURA heater in
684 Russia as a transmitter and the UTR-2 radio telescope in Ukraine as a receiver [Rodrigues,
685 2013]. The study was not comprehensive, and the findings were neither conclusive nor
686 well documented.

687 Most recently, solar radar experiments were attempted repeatedly at Jicamarca during a
688 multi-year study [Coles *et al.*, 2006]. An unsuccessful attempt to observe solar echoes at
689 Jicamarca was actually made back in 1964, but it was not documented (personal communica-
690 tion, K. Bowles, B. Balsley, and D. Farley). In the recent experiments, the average power

691 and antenna gain were about 112 kW and 41.6 dB, respectively. After a thorough statistical
 692 analysis of the data, no clear, unambiguous echoes were found, and the upper bound on the
 693 solar cross section was reduced to a figure below that implied El Campo observations. The
 694 implication of the study was that the echoes reported from El Campo might have been spu-
 695 rious and associated with solar radio bursts rather than radar reflections. This conclusion
 696 is controversial and does not explain the Arecibo results.

697 **5.6.2. Experimental demands**

698 As mentioned above, for solar, magnetospheric, and plasmaspheric studies, the radar
 699 wavelength must be longer than the plasma Debye length. This places a premium on low
 700 radar frequencies which overrides the penalty of increased sky noise. However, the radar
 701 frequency should not fall below the maximum usable frequency (MUF) since that would
 702 invite radar clutter from sky waves. The ideal frequency is therefore between 40–50 MHz.
 703 Some additional frequency considerations are discussed below.

The simple figure of merit described below is not appropriate for optimizing solar radar experiments in which the transmit and receive antenna specifications need to be considered separately. Optimum array sizes are determined by the power budget for solar echoes. The radar equation can be used to estimate the received signal flux:

$$S_r = P_t G_t L_p \sigma_r / (4\pi r^2)^2 \quad (2)$$

where P_t is the transmitted power, G_t is the gain of the transmitting antenna, L_p is the two-way loss factor for absorption in the lower corona, σ_r is the solar radar cross section,

and r is the solar distance. The noise flux is similarly given by

$$S_s = KT_s\Omega_s B/\lambda^2 \quad (3)$$

where K is Boltzmann's constant, T_s is the solar noise temperature, B is the bandwidth, and λ is the wavelength. The symbol Ω_s is the solid angle subtended by the Sun. It is assumed here that the Sun nearly (but not entirely) fills the field of view of the radar and that all of the noise sources outside the Sun may be neglected. Taking the ratio of Eqs. 2 and 3 gives the anticipated signal-to-noise ratio

$$\text{SNR} = P_t A_t L_p \epsilon_s / (4\pi r^2 K T_s B) \quad (4)$$

in which A_t is the transmitting antenna effective area and ϵ_s is the scattering efficiency of the Sun (**the ratio of the scattering cross section to the physical cross section**), which is assumed to be fully illuminated.

Estimating the factors in Eq. 4 is challenging since solar echo detection remains to be demonstrated and since a mode capable of detecting them remains to be defined. The effective bandwidth of the experiments at Jicamarca following coherent processing is 1 kHz. James [1970] estimated the loss factor L_p to be about 3 dB, although that figure is probably an underestimate (see Coles [2004]; Coles *et al.* [2006] and references therein). The noise temperature of the quiet sun at 50 MHz is of the order of 10^6 K, although the actual system noise is dominated by solar radio bursts as discussed below.

The crucial performance metric is the transmitter power-aperture product which sets the flux that can be delivered to the Sun. In order to optimize this flux, the antenna for

717 transmission should be a steerable aperture or filled array at least comparable in size to
 718 Jicamarca's. Steerability is necessary to keep the radar beam trained on the Sun, facilitating
 719 long incoherent integration times.

720 Remarkably, the receive-array size does not enter into the calculation. In fact, the receive
 721 array must be large enough that most of the noise it receives comes from the solar disk itself
 722 and not from the galactic background. This assumption, which is not difficult to satisfy in
 723 practice, is built into eq. 4. Moreover, we have to consider that the main source of noise in
 724 solar radar experiments will be solar radio bursts.

725 Observations of the Sun at meter wavelengths with Culgoora and CLRO have shown
 726 that the various radio burst (Types I, II, III, IV, etc) have at least 20 dB and often 30 dB
 727 higher brightness than the quiet Sun. The most common burst, type III, comes from a small
 728 region and is broadened by scattering in the corona to angular size of order 3 arc min at
 729 80 MHz. When the radar receiver beam covers the whole Sun, as it did in the early solar
 730 radar experiments, these bursts dominate the system noise temperature by a large factor.

731 Accordingly, a solar radar receiver must be able to resolve type III bursts so that the receive
 732 beam can be directed to the quiet Sun between the bursts. In fact it would be preferable
 733 to design the receive beam to have nulls at the position of the type III bursts, implying
 734 the need for a maximum likelihood beam-former. However the antenna must be capable
 735 of resolving the burst in order to put a null on it and to perform imaging with very high
 736 dynamics range [*Oberoi et al.*, 2018; *Mondal et al.*, 2018; *Sharma et al.*, 2018].

737 These considerations suggest that a suitable receiving antenna will be a phased array
 738 with an aperture of order 10 km in diameter and a beam-former that can form multiple

739 simultaneous beams with very low sidelobes. However, special efforts to suppress grating
740 lobes will not be necessary since the Sun is by far the most powerful noise source in the
741 Sky, and very low-noise receivers will not be required. Instead, the receivers must be
742 optimized for high dynamic range and good stability. Good calibration and good stability
743 will be required to minimize sidelobes.

744 **5.6.3. Solar-radar opportunity**

745 The possibility of observing not only the sun but also solar arcs and coronal mass ejec-
746 tions (CMEs) with ground-based radar remains an attractive scientific objective and an
747 important impetus for this project. A solar-radar capability could possibly be used to es-
748 timate the range, bearing, and speed of a CME. Such information could form the basis
749 of practical space weather event forecasts. It could also supply critical information to
750 more conventional model-based forecasts, including information about the coronal mag-
751 netic field inferred from Faraday rotation.

6. Facility capabilities and requirements

752 Table 1 summarizes the capabilities of a geospace radar which would be able to pursue
753 the research objectives described above. The categories in the table are broad, and the
754 delineations are somewhat artificial, as most of the radar's capabilities would be exploited
755 in every avenue of research over time as the research matures. The table does show how
756 progress across a broad span of geospace science would follow from the pursuit of the
757 geospace-radar concept.

758 Most every scientific application requires high peak power of the order of one to several
759 MW. Additional sensitivity would come from high average power or even CW operations
760 involving the transmission of long pulse codes. Sensitivity will be critical for applications
761 where either transmission or reception occurs on subarrays of the main antenna array, for
762 example in MIMO and imaging applications. High average power is important especially
763 for estimating meteoric mass flux and for probing distant targets, the solar corona most
764 acutely. High duty cycles are a cost-effective strategy for achieving high average power
765 and good sensitivity in view of the fact that costs are driven largely by peak power.

766 Multistatic observations are the only way to measure vector drifts unambiguously and
767 are important for every avenue of geospace research except perhaps planetary radar. The
768 contemporary practice of inferring three-dimensional flow fields from monostatic line-of-
769 sight drift measurements is impeding our understanding of the complex dynamics found
770 throughout the upper atmosphere. The ability to track CMEs with multistatic solar radar
771 would provide an incisive tool for space-weather forecasting.

772 Distributed, modular receive arrays supported by multichannel receivers are central to
773 the radio-array concept and the foundation of true radio and radar imaging. More than any
774 other capability, the modern geospace radar would rely upon distributed spatial sensing
775 to unravel space-time ambiguity and reveal the three-dimensional structure of targets and
776 features in the upper atmosphere, the plasmasphere, and the solar corona. While planetary
777 radars derive imaging information from the Doppler shift, interferometry is essential for
778 disambiguating echoes from the northern and southern hemispheres.

779 Both multi-static and distributed modular arrays could be implemented with current tech-
780 nology used in modern radio arrays, e.g., LOFAR, LWA, MWA. To use such systems as
781 receivers of the proposed main transmitter array, the capability to record signals centered
782 around the frequencies of interest is needed. Such capability has been proven already at
783 KAIRA, LOFAR International, and LWA-SV, receiving signals from transmitters operat-
784 ing from a few MHz to 54 MHz. In the case of solar-radar applications, an array of arrays
785 with spacings up to 10 km or so, like LOFAR-core (e.g., *Kontar et al.* [2017]), would be
786 needed. To be able to get both high resolution images of solar radio burst and solar radar
787 echoes, the pre-combined complex signals of each array need to be recorded so that spatial
788 autocorrelation functions are available and, from them, the brightness of solar burst as well
789 as of solar echoes. Complex voltages would be needed to accommodate the transmitter
790 modulation.

791 **Full polarization diversity is absent in all of the current ISRs with the exception of**
792 **Jicamarca. Polarimetry is used there now to measure Faraday rotation which serves**
793 **as means of calibrating ISR power measurements absolutely. Echoes from meteors**
794 **and from the planets can also be polarized due to incidences of multiple scatter. The**
795 **polarization of meteor echoes in particular is an important source of information**
796 **about the scattering mechanism that has been largely overlooked. Looking forward,**
797 **polarimetry could be a rich new source of information about geospace and could**
798 **potentially reveal the magnetic structure in the corona and the solar wind in the case**
799 **of solar radar. Work along these lines is already underway *Salah et al.* [2005]; *Bisi***
800 ***et al.* [2017]; *Lenc et al.* [2017].**

801 Wide-band and multi-frequency capabilities represent another new frontier for discovery
802 science. Solar-radar modes are inherently wide band because the modulation schemes
803 involved use frequency-shift keying (FSK).

804 In cases where the target RCS is large enough, e.g., MST, Meteor, FAIs, and perhaps
805 the Moon, coherent and non-coherent MIMO implementations will be useful. The avail-
806 able high power could be diversified to study such targets with unprecedented horizon-
807 tal and altitude resolution and horizontal coverage. For example, FAIs could be studied
808 with simultaneous multi-static links and aperture synthesis radar imaging by employing
809 interferometric configurations on transmission with diversity (e.g., code) and receiving on
810 multiple receiving sites consisting of single antennas (MISO configurations) or more an-
811 tennas (MIMO). This would facilitate studies of FAIs at different scattering points along
812 the Earth's magnetic field in addition to traditional imaging in just the transverse direction.

7. Concluding Remarks

813 A geospace radar as described in this paper would lead not only to a better understanding
814 and practical utilization of the natural echoes studied with existing radars but also to an
815 appreciation of more challenging targets and regions that are waiting to be explored. Here,
816 we have considered just a few research opportunities starting from the lower atmosphere
817 and arriving at the Sun.

818 Although special emphasis has been devoted to applications related to space-weather
819 research and operations like the early detection of the sources of the most extreme events
820 (i.e., CMEs) and efforts to forecast the day-to-day variability of ionospheric irregularities

821 (e.g., ESF), a geospace radar would contribute to other basic and applied research areas.
822 To name a few: plasma instabilities in the plasmasphere as well as the valley region, turbu-
823 lence and layering processes in the MST region, meteor composition, meteor mass, solar
824 plasma processes, etc. Furthermore, the receive array portion of the radar could be used
825 passively for radio astronomy or be paired with HF sounders for multistatic ionospheric
826 sounding experiments. **The solar-radar application remains the most compelling sin-**
827 **gle science objective, however, being a compelling new avenue of remote sensing in its**
828 **own right and holding the promise for end-to-end space-weather forecasting.**

829 As with any large endeavor, the implementation and subsequent operation of a geospace
830 radar would require a multidisciplinary approach. The effort would necessarily involve,
831 for example, signal processing, statistical inverse theory, software radio, big data han-
832 dling/processing, machine learning, energy efficient practices, etc. That is, it would require
833 the participation and interaction of a workforce encompassing key disciplines of society
834 drawn from science, technology, engineering, and mathematics (STEM) working toward
835 societal security and prosperity.

836 **Acknowledgments.** The Jicamarca Radio Observatory is a facility of the Instituto Ge-
837 ofísico del Perú operated with support from NSF award AGS-1732209 to Cornell. Data in
838 this manuscript can be found in the Madrigal database at <http://www.openmadrigal.org>.

References

839 Bastian, T. S., Progress on the Frequency Agile Solar Radiotelescope, Proc. SPIE 4853,
840 Innovative Telescopes and Instrumentation for Solar Astrophysics, 11 February, 2003.

841 Bastian, T. S., Low-frequency solar radiophysics with LOFAR and FASR, *Planetary and*
842 *Space Science*, 52, 1381–1389, 2004.

843 Beynon, W. J. G., and P. J. S. Williams, Incoherent scatter of radio waves from the iono-
844 *sphere, Reports on Progress in Phys.*, 41, 909, 1978.

845 Bisi, M. M., et al., Observations and Analyses of Heliospheric Faraday Rotation of a Coro-
846 *nal Mass Ejection (CME) Using the LOw Frequency ARray (LOFAR) and Space-Based*
847 *Imaging Techniques, in EGU General Assembly Conference Abstracts*, vol. 19, p. 13243,
848 2017.

849 Chau, J. L., R. F. Woodman, and F. R. Galindo, Sporadic meteor sources as observed by
850 the Jicamarca high-power large-aperture VHF radar, *Icarus*, 188 (1), 162–174, 2007.

851 Chau, J. L., R. F. Woodman, M. A. Milla, and E. Kudeki, Naturally enhanced ion-line
852 spectra around the equatorial 150-km region, *Ann. Geophys.*, 27, 933–942, 2009.

853 Chau, J. L., D. McKay, J. P. Vierinen, C. La Hoz, T. Ulich, M. Lehtinen, and R. Latteck,
854 Multi-static spatial and angular studies of polar mesospheric summer echoes combining
855 maarsy and kaira, *Atmospheric Chemistry and Physics*, 18, 9547–9560, 2018a.

856 Chau, J. L., J. M. Urco, J. P. Vierinen, R. A. Volz, M. Clahsen, N. Pfeffer, and J. Traut-
857 ner, Novel specular meteor radar systems using coherent mimo techniques to study
858 the mesosphere and lower thermosphere, *Atmospheric Measurement Techniques Dis-*
859 *cussions, 2018*, 1–23, 2018b.

860 Coles, W. A., Solar radar, in *Solar and Space Weather Radiophysics*, edited by D. E. Gary
861 and C. Keller, chap. 16, Springer, New York, 2004.

862 Coles, W. A., J. K. Harmon, M. P. Sulzer, J. L. Chau, and R. F. Woodman, An
863 upper bound on the solar radar cross section at 50 MHz, *J. Geophys. Res.*, *111*,
864 doi:10.1029/2005JA011,416, 2006.

865 Cranmer, M. D., et al., Bifrost: A python/c++ framework for high-throughput stream pro-
866 cessing in astronomy, *Journal of Astronomical Instrumentation*, *06*, 1750,007, 2017.

867 Dougherty, J. P., and D. T. Farley, A theory of incoherent scattering of radio waves by a
868 plasma, *Proc. Roy. Soc. A* *259*, 79–99, 1960.

869 Dougherty, J. P., and D. T. Farley, A theory of incoherent scattering of radio waves by a
870 plasma, 3, scattering in a partly ionized gas, *J. Geophys. Res.*, *68*, 5473–5486, 1963.

871 Ellingson, S. W., et al., The LWA1 Radio Telescope, *IEEE Trans. Antennas and Propaga-*
872 *tion*, *5*, 2540–9, 2012.

873 Eshleman, V. R., R. C. Barthle, and P. B. Gallagher, Radar echoes from the Sun, *Science*,
874 *131*, 329–332, 1960.

875 Fallows, R., et al., Broadband meter-wavelength observations of ionospheric scintillation,
876 *Journal of Geophysical Research: Space Physics*, *119*, 10–544, 2014.

877 Farley, D. T., Early incoherent scatter observations at Jicamarca, *J. Atmos. Terr. Phys.*, *53*,
878 665–675, 1991.

879 Farley, D. T., J. P. Dougherty, and D. W. Barron, A theory of incoherent scattering of radio
880 waves by a plasma, 2, Scattering in a magnetic field, *Proc. R. Soc., London Ser. A*, *263*,
881 238–258, 1961.

882 Fejer, J. A., Scattering of radio waves by an ionized gas in thermal equilibrium, *Can. J.*
883 *Phys.*, *38*, 1114–1133, 1960.

884 Fejer, J. A., Scattering of radio waves by an ionized gas in thermal equilibrium in the
885 presence of a uniform magnetic field, *Can. J. Phys.*, pp. 716–740, 1961.

886 Hagfors, T., Density fluctuations in a plasma in a magnetic field, with applications to the
887 ionosphere, *J. Geophys. Res.*, 66, 1699–1712, 1961.

888 Hocking, W., A review of mesospherestratospheretroposphere (mst) radar developments
889 and studies, circa 19972008, *Journal of Atmospheric and Solar-Terrestrial Physics*, 73,
890 848 – 882, 2011, scientific Results from Networked and Multi-instrument studies based
891 on MST Radar.

892 Hysell, D. L., and J. L. Chau, Optimal aperture synthesis radar imaging, *Radio Sci.*, 41,
893 10.1029/2005RS003,383, RS2003, 2006.

894 Hysell, D. L., F. S. Rodrigues, J. L. Chau, and J. D. Huba, Full profile incoherent scatter
895 analysis at Jicamarca, *Ann. Geophys.*, 26, 59–75, 2008.

896 Hysell, D. L., M. F. Larsen, and M. P. Sulzer, High time and height resolution neutral
897 wind profile measurements across the mesosphere/lower thermosphere region using the
898 Arecibo incoherent scatter radar, *J. Geophys. Res.*, 119, DOI: 10.1002/2013JA019,621,
899 2014.

900 Hysell, D. L., J. Vierinen, and M. P. Sulzer, On the theory of the incoherent scatter gyro-
901 lines, *Radio Sci.*, 52, 723–730, doi:10.1002/2017RS006,283, 2017.

902 James, J. C., Radar echoes from the Sun, *IEEE Trans. Antennas Propag.*, AP-12, 876–891,
903 1964.

904 James, J. C., El Campo solar radar data and system design notes, *Tech. Rep.* 70-2, MIT
905 Cent. of Space Res., Cambridge, Mass, 1970.

906 Kero, A., J. Vierinen, D. McKay-Bukowski, C.-F. Enell, M. Sinor, L. Roininen, and
907 Y. Ogawa, Ionospheric electron density profiles inverted from a spectral riometer mea-
908 surement, *Geophysical Research Letters*, 41, 5370–5375, 2014.

909 Kero, J., C. Szasz, T. Nakamura, D. D. Meisel, M. Ueda, Y. Fujiwara, T. Terasawa,
910 H. Miyamoto, and K. Nishimura, First results from the 20092010 mu radar head echo
911 observation programme for sporadic and shower meteors: the orionids 2009, *Monthly*
912 *Notices of the Royal Astronomical Society*, 416, 2550–2559, 2011.

913 Khotyaintsev, M. V., Theory of solar radar experiments: Combination scattering by
914 anisotropic Langmuir turbulence, Ph.D. thesis, Uppsala University, Uppsala, Sweden,
915 2005.

916 Kontar, E. P., S. Yu, A. A. Kuznetsov, A. G. Emslie, B. Alcock, N. L. S. Jeffrey, V. N.
917 Melnik, N. H. Bian, and P. Subramanian, Imaging spectroscopy of solar radio burst fine
918 structures, *Nature Communications*, pp. 1–9, 2017.

919 Kudeki, E., and M. A. Milla, Incoherent scatter spectral theories—Part I: A general frame-
920 work and results for small magnetic aspect angles, *IEEE Transactions on Geoscience*
921 and *Remote Sensing*, 49, 315–328, 2011.

922 Lehtinen, M. S., Statistical theory of incoherent scatter radar measurements, *Tech. Rep.*
923 86/45, Eur. Incoherent Scatter Sci. Assoc., Kiruna, Sweden, 1986.

924 Lenc, E., et al., The challenges of low-frequency radio polarimetry: Lessons from the
925 Murchison Widefield Array, *Publications of the Astronomical Society of Australia*, 34,
926 e040, 2017.

927 Loi, S. T., et al., Real-time imaging of density ducts between the plasmasphere and iono-
928 sphere, *J. Geophys. Res.*, 42, 10.1002/2015GL063,699, 2015.

929 Maekawa, Y., S. Fukao, M. Yamamoto, M. D. Yamanaka, T. Tsuda, S. Kato, and R. F.
930 Woodman, First observation of the upper stratospheric vertical winds observed by the
931 Jicamarca VHF radar, *Geophys. Res. Lett.*, 20, 2235, 1993.

932 McCrea, I., et al., The science case for the eiscat_3d radar, *Progress in Earth and Planetary
933 Science*, 2, 21, 2015.

934 McKay-Bukowski, D., et al., Kaira: The kilpisjärvi atmospheric imaging receiver arraysys-
935 tem overview and first results, *IEEE Transactions on Geoscience and Remote Sensing*,
936 53, 1440–1451, 2015.

937 Milla, M. A., and E. Kudeki, Incoherent scatter spectral theories–Part II: Modeling the
938 spectrum for modes propagating perpendicular to \vec{B} , *IEEE Transactions on Geoscience
939 and Remote Sensing*, 49, 329–345, 2011.

940 Milla, M. A., E. Kudeki, J. L. Chau, and P. M. Reyes, A multi-beam incoherent scatter
941 radar technique for the estimation of ionospheric electron density and t_e/t_i profiles at
942 jicamarca, *Journal of Atmospheric and Solar-Terrestrial Physics*, 105-106, 214–229,
943 2013.

944 Mondal, S., A. Mohan, D. Oberoi, L. Benkevitch, C. J. Lonsdale, J. Morgan, M. Crowley,
945 and I. Cairns, First results from automated imaging routine for compact arrays for radio
946 sun, *Proceedings of the International Astronomical Union*, 13, 159–160, 2018.

947 Nicolls, M. J., R. H. Varney, S. L. Vadas, P. A. Stamus, C. J. Heinselman, R. B. Cos-
948 grove, and M. C. Kelley, nfluence of an inertia-gravity wave on mesospheric dynamics:

949 A case study with the Poker Flat Incoherent Scatter Radar, *J. Geophys. Res.*, p. doi:
950 10.1029/2010JD014042, 2010.

951 Oberoi, D., et al., Solar science at metric radio wavelengths: Coming of age, in *IAU Sym-*
952 *posium*, edited by D. Banerjee, J. Jiang, K. Kusano, and S. Solanki, vol. 340 of *IAU*
953 *Symposium*, pp. 145–146, 2018.

954 Oppenheim, M. M., G. Sugar, N. O. Slowey, E. Bass, J. L. Chau, and S. Close, Remote
955 sensing lower thermosphere wind profiles using non-specular meteor echoes, *Geophys.*
956 *Res. Lett.*, 36, doi:10.1029/2009GL037,353, 2009.

957 Parrish, A., Solar radar experiments, 1967, *Tech. rep.*, Center for Radiophysics and Space
958 Physics, Cornell University, 1968.

959 Perkins, F. W., E. E. Salpeter, and K. O. Yngvesson, Incoherent scatter from plasma oscil-
960 lations in the ionosphere, *Phys. Rev. Lett.*, 14, 579–581, 1965.

961 Rodrigues, P., Radar studies of the solar corona: A review of experiments using HF wave-
962 lengths, in *Radio Astronomy at Long Wavelengths*, edited by R. G. Stone, K. W. Weiler,
963 M. L. Goldstein, and J. L. Bougerat, pp. 155–165, American Geophysical Union, 2013.

964 Rogers, A. E., and J. D. Bowman, Spectral index of the diffuse radio background measured
965 from 100 to 200 mhz, *The Astronomical Journal*, 136, 641, 2008.

966 Rosenbluth, M. N., and N. Rostocker, Scattering of electromagnetic waves by a nonequi-
967 librium plasma, *Phys. Fluids*, 5, 776–788, 1962.

968 Salah, J. E., C. J. Lonsdale, D. Oberoi, R. J. Cappallo, and J. C. Kasper, Space weather
969 capabilities of low frequency radio arrays, *Proc. SPIE 5901, Solar Physics and Space*
970 *Weather Instrumentation*, 59010G, doi: 10.1117/12.613,448, 2005.

971 Salpeter, E. E., Electron density fluctuations in a plasma, *Phys. Rev.*, 120, 1528–1535,
972 1960.

973 Salpeter, E. E., Plasma density fluctuations in a magnetic field, *Phys. Rev.*, 122, 1663–1674,
974 1961.

975 Schult, C., G. Stober, D. Janches, and J. L. Chau, Results of the first continuous meteor
976 head echo survey at polar latitudes, *Icarus*, 297, 1 – 13, 2017.

977 Sharma, R., D. Oberoi, and M. Arjunwadkar, Quantifying weak nonthermal solar radio
978 emission at low radio frequencies, *The Astrophysical Journal*, 852, 69, 2018.

979 Stober, G., and J. L. Chau, A multistatic and multifrequency novel approach for specular
980 meteor radars to improve wind measurements in the MLT region, *Radio Science*, 50,
981 431–442, 2015, 2014RS005591.

982 Stober, G., J. L. Chau, J. Vierinen, C. Jacobi, and S. Wilhelm, Retrieving horizontally
983 resolved wind fields using multi-static meteor radar observations, *Atmospheric Mea-*
984 *surement Techniques Discussions*, 2018, 1–25, 2018.

985 Taylor, G., Thermospheric neutral wind measurement using the lwa1 and the afrl
986 digisonde, *Tech. rep.*, NEW MEXICO UNIV ALBUQUERQUE DEPT OF PHYSICS
987 AND ASTRONOMY, 2014.

988 Urco, J. M., J. L. Chau, M. A. Milla, J. P. Vierinen, and T. Weber, Coherent mimo to
989 improve aperture synthesis radar imaging of field-aligned irregularities: First results at
990 jicamarca, *IEEE Transactions on Geoscience and Remote Sensing*, PP, 1–11, 2018.

991 Urco, J. M., J. L. Chau, T. Weber, and R. Latteck, Enhancing the spatiotemporal features
992 of polar mesosphere summer echoes using coherent mimo and radar imaging at maarsy,

993 *Atmospheric Measurement Techniques*, 12, 955–969, 2019.

994 van Haarlem, M. P., J. Blo, and J. Otherblo, LOFAR: The low-frequency array, *Astronomy*
995 and *Astrophysics*, 556, A2, 2013.

996 Vierinen, J., D. McKay-Bukowski, M. S. Lehtinen, A. Kero, and T. Ulich, Kilpisjärvi
997 atmospheric imaging receiver arrayfirst results, in *Phased Array Systems & Technology*,
998 2013 IEEE International Symposium on, pp. 664–668, IEEE, 2013.

999 Vierinen, J., J. L. Chau, N. Pfeffer, M. Clahsen, and G. Stober, Coded continuous wave
1000 meteor radar, *Atmospheric Measurement Techniques*, 9, 829–839, 2016.

1001 Vierinen, J., T. Tveito, B. Gustavsson, S. Kesaraju, and M. Milla, Radar images of the
1002 moon at 6-meter wavelength, *Icarus*, 297, 179–188, 2017.

1003 Virtanen, I., D. McKay-Bukowski, J. Vierinen, A. Aikio, R. Fallows, and L. Roininen,
1004 Plasma parameter estimation from multistatic, multibeam incoherent scatter data, *Journal*
1005 of *Geophysical Research: Space Physics*, 119, 10–528, 2014.

1006 Woodman, R. F., Incoherent scattering of electromagnetic waves by a plasma, Ph.D. thesis,
1007 Harvard University, 1967.

1008 Woodman, R. F., and J. L. Chau, Antenna compression using binary phase coding, *Radio*
1009 *Sci.*, 36, 45, 2001.

1010 Woodman, R. F., and A. Guillén, Radar observations of winds and turbulence in the strato-
1011 sphere and mesosphere, *J. Atmos. Sci.*, 31, 493–505, 1974.

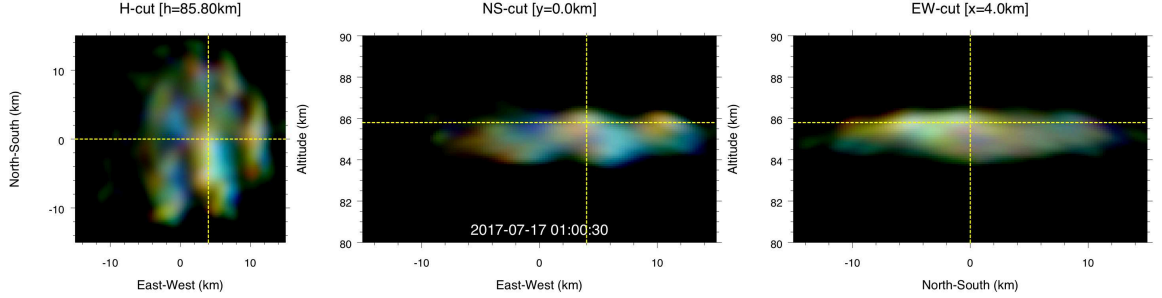


Figure 1. Example of 3D PMSE images obtained with a combination of MaxENT radar imaging and time-diversity MIMO techniques using the MAARSY radar: (a) horizontal cut at 85.80 km, (b) altitude versus zonal cut, and (c) altitude versus meridional cut. Doppler velocity, spectral width, and intensity are color-coded in the images. Adapted from *Urco et al. [2019]*

Mon Sep 4 09:12:44 2017

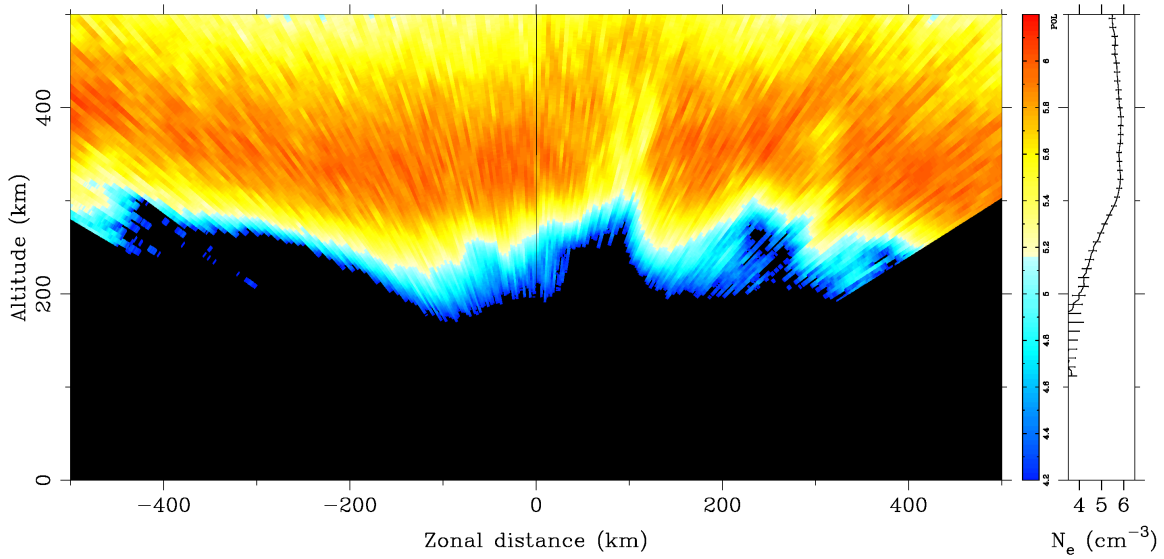


Figure 2. Incoherent scatter observations of large-scale plasma density irregularities and plume-like depletions associated with equatorial spread F made with the ALTAIR radar. The data were acquired with antenna scans directed a few degrees away from perpendicular to the geomagnetic field.

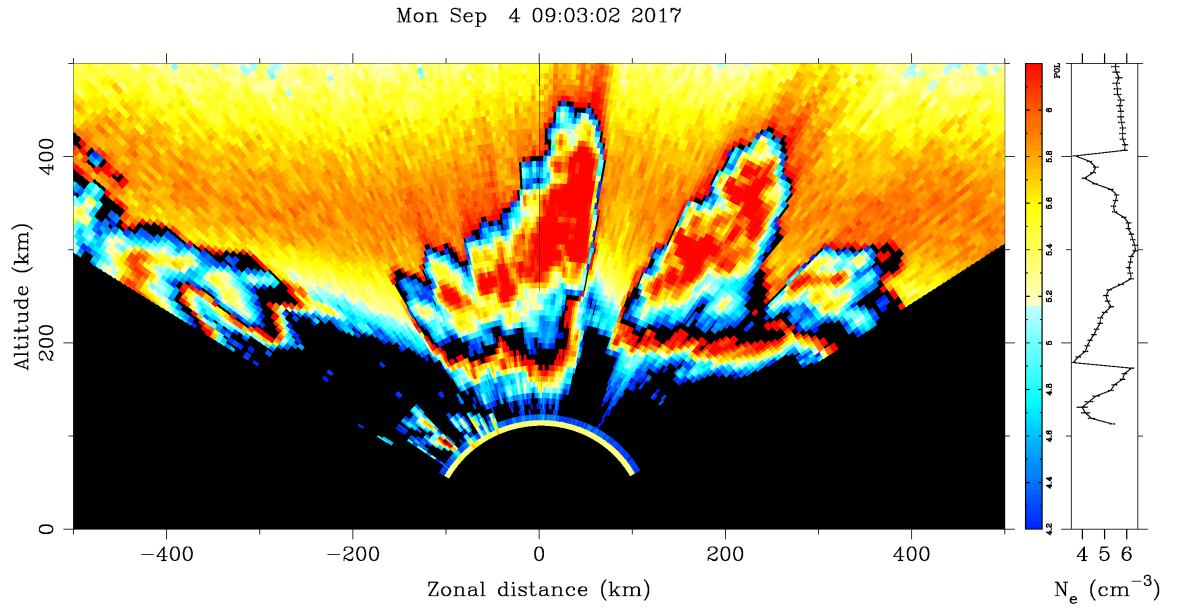


Figure 3. Radar observations of irregularities associated with equatorial spread F made with ALTAIR antenna scans directed perpendicular to the geomagnetic field. Coherent scatter can be observed in the most deeply depleted parts of the F region. In this figure, the coherent scatter is automatically attenuated by 20 dB for plotting.

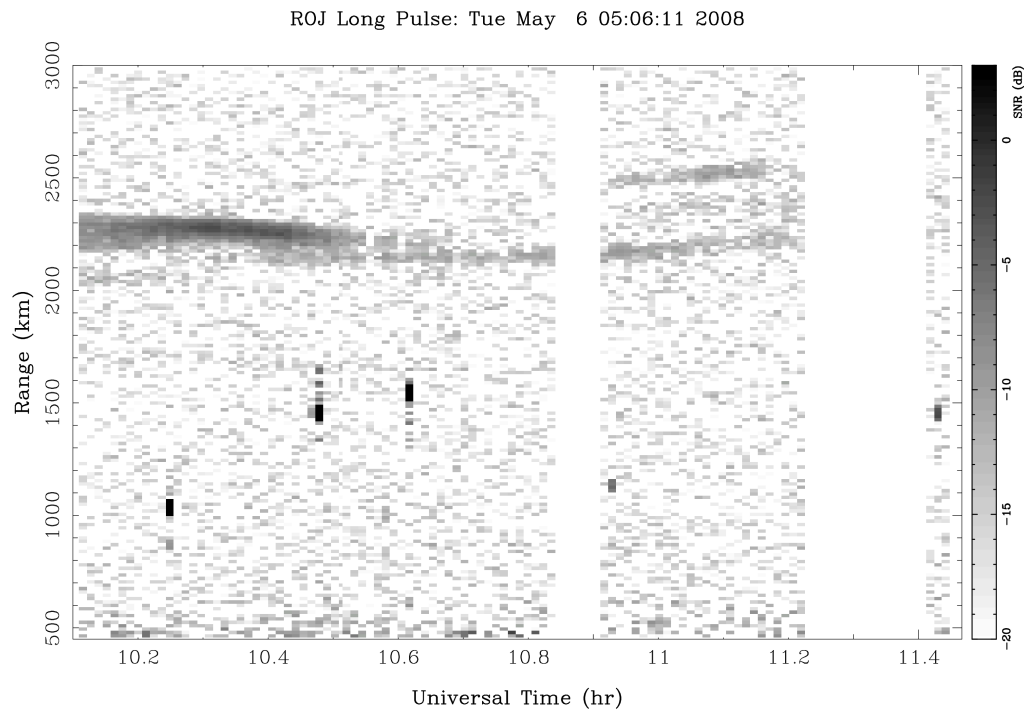


Figure 4. Coherent scatter signal-to-noise ratio derived from topside observations at Jicamarca in the pre-dawn sector. For this figure, radar clutter due to satellites and debris most evident between 1000-1500 km has not been removed.

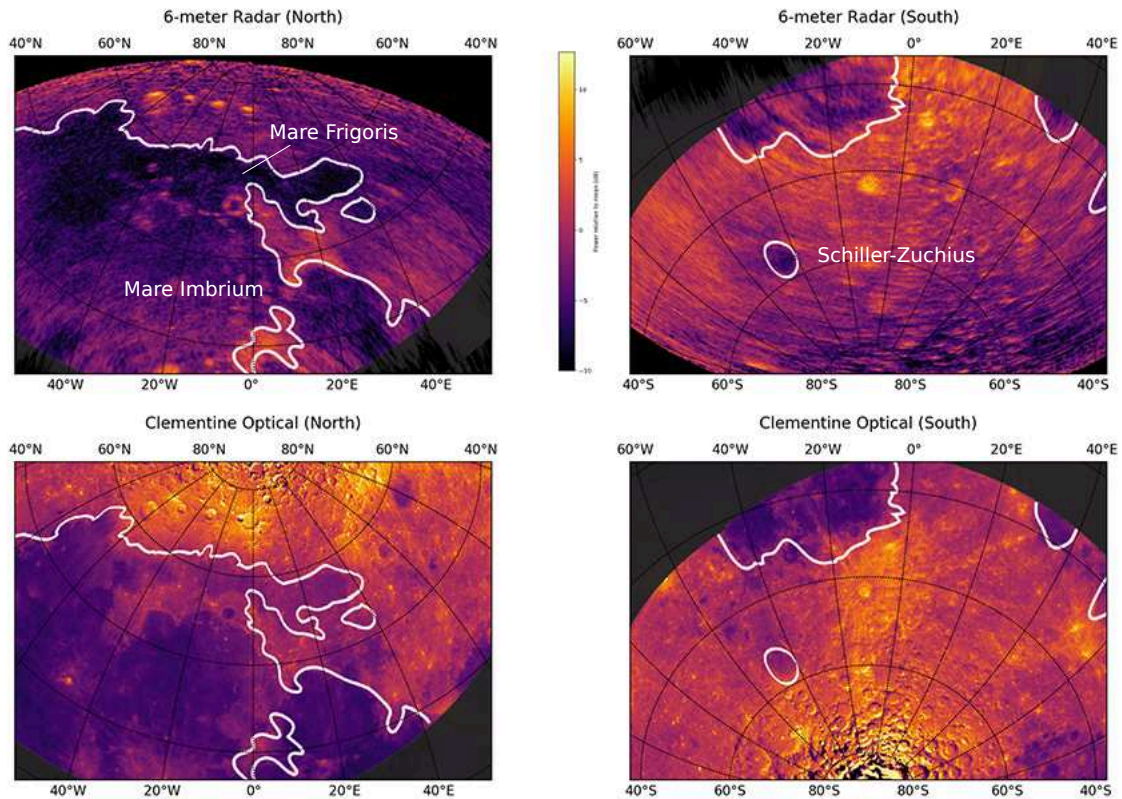


Figure 5. Top: 6-meter wavelength radar map of the Moon derived from Jicamarca data with polarization orthogonal to the specular polarization. Bottom: Clementine optical image of the Moon.

Capability	MST	Meteor	ISR	FAIs	Plasmasphere	Planetary	Solar
High peak power	✓	✓	✓		✓	✓	✓
High duty cycle	✓	✓	✓	✓	✓	✓	✓
Multistatic	✓	✓	✓	✓	✓		✓
Distributed	✓	✓	✓	✓	✓	✓	✓
Polarimetric		✓	✓			✓	✓
Wide band	✓	✓					✓
MIMO	✓	✓		✓			

Table 1. Capabilities versus potential applications.